Vapour-liquid-solid growth of ZnO-ZnMgO core–shell nanowires by gold-catalysed molecular beam epitaxy

OPEN ACCESS
IOP Publishing
Nanotechnology
Nanotechnology 30 (2019) 194001 (5pp)
https://doi.org/10.1088/1361-6528/ab011c

Vapour-liquid-solid growth of ZnO-ZnMgO core–shell nanowires by gold-catalysed molecular beam epitaxy

O W Kennedy[1], E R White[2], M S P Shaffer[2] and P A Warburton[1,3]

[1] London Centre for Nanotechnology, UCL, 17-19 Gordon Street, London, WC1H 0AH, United Kingdom
[2] Departments of Chemistry and Materials, Imperial College London, Imperial College Road, London, SW7 2AZ, United Kingdom

E-mail: p.warburton@ucl.ac.uk

Received 31 October 2018, revised 8 January 2019
Accepted for publication 23 January 2019
Published 22 February 2019

Abstract

Nanowire heterostructures, combining multiple phases within a single nanowire, modify functional properties and offer a platform for novel device development. Here, ZnO/ZnMgO core–shell nanowires are grown by molecular beam epitaxy. At growth temperatures above 750 °C, Mg diffuses into ZnO making heterostructure growth impossible; at lower shell-growth temperatures (500 °C), the core–shell structure is retained. Even very thin ZnMgO shells show increased intensity photoluminescence (PL) across the ZnO band-gap and a suppression in defect-related PL intensity, relative to plain ZnO nanowires. EDX measurements on shell thickness show a correlation between shell thickness and core diameter which is explained by a simple growth model.

Keywords: nanowires, ZnO, heterostructure, MBE

(Some figures may appear in colour only in the online journal)

1. Introduction

Nanowire heterostructures, where multiple chemistries are combined within a single nanowire, allow for the modification and enhancement of nanowire functional properties [1–3]. There are broadly two types of nanowire heterostructure, defined by the quasi-one-dimensional nanowire geometry: axial heterostructures (where the chemistry changes along the axis of the nanowire) and radial or core–shell heterostructures (where the chemistry changes in a direction perpendicular to the nanowire axis).

Such heterostructures are typically grown in a step-wise manner: a nanowire of one material is grown first and then the growth conditions are changed to deposit a chemically distinct secondary material. Nanowires are frequently grown via variants of the so-called vapour liquid solid (VLS) mechanism. Axial growth occurs when a liquid particle at the nanowire tip absorbs reactants, becomes super-saturated and thus deposits a crystalline layer at the nanowire tip. Radial growth occurs when mobile reactants adsorbed on the sample surface react before reaching the liquid particle and are deposited on the sidewalls of the nanowire. By varying the growth conditions the relative rate of these alternatives may be controlled. This approach provides, in principle, a straightforward way to grow different types of heterostructure with a high degree of control.

$Zn_{1-x}Mg_xO$ is a wide band gap semiconductor in which the band gap, E_g increases with x, the Mg concentration, whilst maintaining a wurtzite structure. The room temperature band gap is determined [4] to depend on x as $E_g = 3.30 + 2.36x$. At large values of x, the rock-salt phase of MgO starts to segregate, although the precise value of x depends on film thickness and the substrate; films with $x = 0.61$ have been reported without segregation [5]. ZnO/ZnMgO heterostructures, therefore, allow band-gap misaligned epitaxial heterointerfaces to form. ZnO/ZnMgO nanowire heterostructures have been previously grown by

[3] Author to whom any correspondence should be addressed.

metal organic vapour phase epitaxy [6–8] and pulsed laser deposition [9]. In these heterostructures, ZnO quantum wells are sandwiched between ZnMgO layers leading to quantum confinement. In this case, no catalyst was used and growth is likely driven by vapour–solid mechanisms. Thermal evaporation has been used to grow core–shell $Zn_{1-x}Mg_xO/Zn_{1-y}Mg_yO$ with $y > x$ where the core had wurtzite and the shell cubic crystal structures, likely due to phase segregation [10]. ZnO/MgO core–shell nanowires have also been grown by MBE with VLS growth [11]. But again, the shells had the rock-salt structure precluding an epitaxial interface around the full wurtzite core.

In this manuscript, ZnO/ZnMgO core–shell nanostructures are grown via a two-stage VLS process based on molecular beam epitaxy, in the form of 'forests' deposited on a substrate. The effects of growth conditions on core/shell dimensions, and interface sharpness are explored with transmission electron microscopy. The intensity of photoluminescence (PL) is used to study the modified properties of the heterostructure nanowires.

2. Experimental

ZnO nanowires are grown by gold-catalysed plasma-assisted MBE as previously reported [12, 13]. *C*-axis sapphire coated with a ~3 nm film of thermally evaporated gold is used as the substrate. Upon heating the sample, the gold melts and dewets from the substrate forming self–assembled liquid nanoparticles. Elemental Zn flux with beam equivalent pressure (BEP) $\sim 3 \times 10^{-7}$ Torr and an oxygen plasma (300 W power, flow of 5×10^{-8} $m^3 s^{-1}$) are directed towards the sample. The gold nanoparticles act as reservoirs for incident Zn and O radicals. Upon supersaturation of the gold nanoparticle a layer of ZnO forms on the base of the nanoparticle resulting in axial nanowire growth by the VLS mechanism. ZnMgO is grown by introducing an elemental Mg flux with a BEP typically 1%–10% of the Zn BEP whilst maintaining the Zn flux and oxygen plasma. Nanowires grown by this technique form forests of nanowires with lengths 0.5–2 μm and diameters 20–100 nm.

Nanowires were characterized by room temperature ensemble PL using a He/Cd laser with an excitation wavelength of 325 nm using a Renishaw fluorescence microscope. The fluorescence microscope has a spot size of approximately 2 μm and so simultaneously addresses approximately 10 nanowires as well as other material not growing in the nanowire geometry. However, similar PL spectra were acquired at multiple locations confirming consistent behaviour. Scanning transmission electron microscope (STEM) and energy dispersive x-ray spectrometry (EDX) measurements were performed in a JEOL 2100Plus. Nanowires were dispersed onto transmission electron microscope (TEM) grids (gold grids with holey carbon and a 2 nm amorphous carbon film) by sonicating as-grown nanowires in 2-propanol causing nanowires to break off and become dispersed. The nanowire dispersion was then pipetted onto the TEM grids and allowed to evaporate.

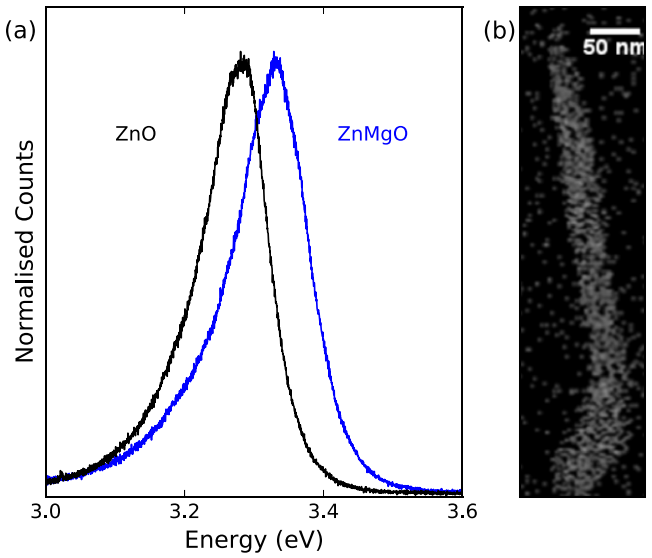

Figure 1. (a) Normalised ensemble PL spectrum of nanowires grown to form axial heterostructures (blue) with plain ZnO nanowire sample for reference (black). (b) EDX map of Mg counts in a representative nanowire showing approximately uniform Mg concentration throughout the nanowire.

3. Results

3.1. Axial heterostructures

First, unsuccessful attempts to grow axial heterostructure nanowires are reported since the results highlight some constraints which must be considered when growing radial heterostructure nanowires. ZnO nanowires were grown as described above for one hour at a sample temperature of 750 °C. After the first hour of growth, an Mg flux of 5.9×10^{-9} Torr (corresponding to 1.6% of the Zn flux) was introduced while maintaining the Zn and O fluxes.

ZnMgO growth was continued for another hour (two hours total growth). Upon completion, Zn and Mg shutters were closed and the oxygen flow for the plasma terminated. In principle (although as shown later not in practice), this regime is expected to produce a nanowire where the lower-half is ZnO and the upper-half is ZnMgO.

PL measurements were performed on ensembles of many of such nanowires (blue curve figure 1(a)). The PL spectrum shows a single peak with maximum counts at 3.33 eV. If heterostructure nanowires had been successfully grown two peaks, one from ZnO and another from the wider-gap ZnMgO, would be expected. The PL spectrum of pure ZnO nanowires grown as a control, without the introduction of magnesium (black curve figure 1(a)) also shows a single peak with a maximum at 3.28 eV. The shift in the PL peak observed from the (intended) axial heterostructures indicates the presence of a homogenised ZnMgO only. The band-gap dependence on x from [4] implies Mg concentration in the heterostructures of ~1% close to the fractional Mg flux and significantly below the solubility limit of Mg in ZnO which can be up to 33% [4].

EDX maps show the Mg distribution within nanowires from this growth run (e.g. figure 1(b)). The EDX maps show that, rather than having discrete regions of ZnO and ZnMgO, magnesium is quite uniformly distributed throughout the nanowire. This observation is consistent with the PL measurement showing only a single peak at energies corresponding to ZnMgO.

Clearly, in this case, a homogeneous, tertiary, nanowire grows instead of an axial heterostructure. At elevated temperatures (750 °C here), in addition to incorporation through the metal catalyst, Mg may also diffuse through the sidewalls into the already-grown-ZnO. This thermal diffusion means that during the ZnMgO growth phase, the ZnO is annealed in a Mg flux, Mg migrates into the ZnO and ZnMgO is formed. Mg diffusion has been reported upon annealing thin films of supersaturated ZnMgO where a rock-salt phase segregates out and ZnO/ZnMgO heterostructures which form uniform ZnMgO films with a lower Mg concentration [14]. Here, instead, the diffusion of adsorbed elemental Mg into the ZnO lattice resulting in uniform doping is shown.

An obvious solution to grow axial heterostructures is to conduct the second growth phase at a lower sample temperature. However, reducing the temperature much below 750 °C causes the gold catalyst particles to solidify and terminates axial growth. It therefore seems that ZnO/ZnMgO axial heterostructures may not be grown by gold-catalysed MBE. These considerations show that despite the large amount of control offered by VLS growth in MBE, the multiple processes occurring in nanowire growth makes heterostructure growth a challenge. An alternative strategy may be to use a metal catalyst with a lower melting point such as tin which has been used [15] to catalyse VLS ZnO nanowire growth at 550 °C–600 °C.

3.2. Radial heterostructures

At lower sample temperatures, although the gold catalyst solidifies terminating axial growth, side-wall growth may continue. Therefore, a different growth procedure was used to grow core–shell heterostructure nanowires. First ZnO nanowires were grown for ∼2 h as described in the experimental section. These nanowires form the cores of the core–shell structure. The sample temperature was then reduced from 750 °C to 500 °C and the oxygen plasma flow reduced from 5.0×10^{-8} $m^3\,s^{-1}$ to 3.3×10^{-8} $m^3\,s^{-1}$. Lower oxygen pressure has been observed to terminate axial growth and result in uniform coverage of the sample with new material, beneficial for core–shell structures. The same Zn flux and also a Mg flux with BEP 2.9×10^{-8} Torr i.e. approximately 10% of the Zn flux was introduced, recommencing growth. The shell was grown for various durations before closing the effusion cell shutters, cooling the sample and terminating growth. Two such samples are considered with shells grown for 630s and 9000s, labelled sample A and B respectively.

Ensemble PL measurements are performed on both samples (figure 2(a)). Both samples show a peak at energies corresponding to the ZnO band gap (∼3.30 eV) with similar amplitudes. The amplitudes of these peaks are directly

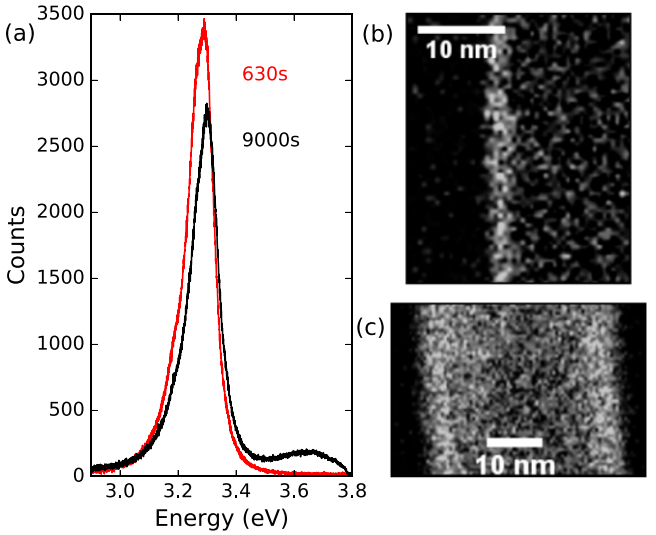

Figure 2. (a) PL spectra of sample A (red) and B (black) where the shell growth occurs for 630s (9000s) for sample A (B). EDX maps of Mg distribution (b) near the edge of a nanowire from sample A and (c) across the full width of a nanowire from sample B.

comparable as data is collected on the same day with identical laser power and collection durations. Sample A shows only luminescence at these energies whereas sample B shows a distinct PL peak at higher energies with maximum intensity at 3.64 eV, corresponding to the bandgap of $Zn_{1-x}Mg_xO$ with 14% Mg content. These data indicate that, at least in sample B, both ZnO and ZnMgO are present in the sample. The ZnMgO on this sample has a higher Mg concentration than the ZnMgO from the attempted axial heterostructures due to the larger Mg flux. X-ray diffraction collected from sample B shows no peaks from cubic ZnMgO or MgO indicating that the shells retain the wurtzite phase of the nanowire cores.

The limited spatial resolution of the PL measurements does not give sufficient information to conclude that the nanowires are ZnO/ZnMgO core–shell heterostructures. EDX maps of nanowires from sample A and B were, therefore, collected as shown in figures 2(b), (c) respectively. Although there is no PL signature from ZnMgO in sample A, the EDX map of the edge of a nanowire from sample A (figure 2(b)) shows a significant increase in Mg counts. These nanowires are, therefore, assigned as core–shell structures with thin shells of ZnMgO coating a ZnO wire. For the thicker shells in sample B, the EDX map extending across the entire diameter of a nanowire (figure 2(c)) shows a clear increase in intensity of Mg at both sides of the nanowire. The Mg rich region is thicker in this nanowire than that shown in figure 2(b), as expected given the longer growth.

In STEM-EDX the primary electron beam penetrates the entire nanowire, with minimal scattering. X-rays may be generated at any point as the primary beam passes through the nanowire, meaning that EDX maps are projections of the elemental composition of a 3D object into a 2D map. When imaging with the electron beam perpendicular to the nanowire growth axis, the magnesium composition of a magnesium-rich shell is projected into 2D resulting in significant counts on the nanowire sides and fewer counts in the centre as seen

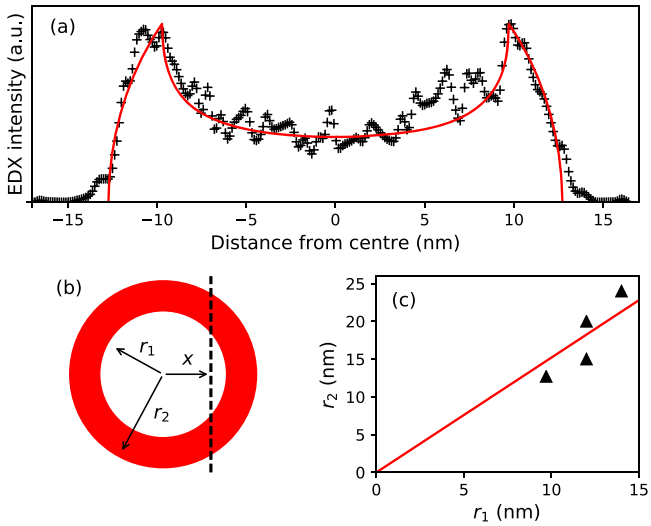

Figure 3. (a) Linescan of EDX intensity for Mg K_α for the EDX map shown in figure 2(c) as a function of distance from nanowire centre. In red is a plot of equation (1) with $r_2 = 12.7$ nm and $r_1 = 9.7$ nm. (b) A schematic showing a shell in red and r_1, r_2 and x from equation (1). The dashed line shows an electron beam penetrating the nanowire generating x-rays. (c) The total radius of the core–shell nanowires r_2 for different nanowires from sample B as a function of the radius of the nanowire core r_1.

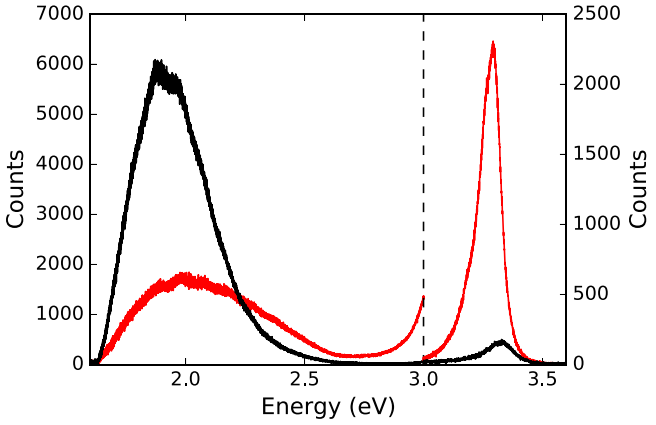

Figure 4. PL spectra of sample A (red) and plain ZnO nanowires (black). Spectra are collected in two measurements, one spanning 1.6–3.0 eV and another 3.0–3.6 eV.

in figure 2. Detailed information could be determined, for example, using more elaborate sample preparation methods to create a FIB section to allow imaging with electrons parallel to the nanowire growth axis [16]. However, with the simpler imaging geometry used in this paper, the cross-section geometry can be estimated by fitting to EDX intensity profiles taken across the nanowire [3].

An ideal core–shell structure with circular cross-section has a cylindrical core encased by a shell of constant thickness and constant chemical composition. The 2D projection of Mg concentration from such a structure is given by

$$I(x) = \begin{cases} 0, & \text{if } |x| > r_2 \\ \sqrt{r_2^2 - x^2}, & \text{if } r_2 > |x| > r_1, \\ \sqrt{r_2^2 - x^2} - \sqrt{r_1^2 - x^2}, & \text{if } |x| < r_1 \end{cases} \quad (1)$$

where r_1 and r_2 are the radii of the core and the whole nanowire respectively and x is the distance from the centre of the nanowire. This geometry is shown in figure 3(b). By fitting the measured EDX Mg intensity to equation (1) the shell thickness $r_2 - r_1$ can be extracted. The EDX line-scan intensity for the nanowire with EDX map shown in figure 2(c) is shown in figure 3(a) with a fit to equation (1) also shown. The extracted value of shell thickness is 3 nm. The good agreement between the profile considering an ideal radial heterostructure, and the EDX profile, indicates that these nanowires are cylindrical core–shell heterostructures.

Using this technique to determine the thickness of nanowire shells, the shell thickness of four different nanowires from sample B is determined (figure 3(c)). For these nanowires, thicker nanowire cores result in thicker shells.

A simple model to explain this trend assumes that a gold film of uniform thickness t de-wets to form spherical catalyst particles of radius $r_1 = (3At/4\pi)^{1/3}$ where A is the area of gold film contributing to the catalyst particle. It is reasonable to assume that flux incident on the same area A will contribute to the nanowire growth from this particle. The gold nanoparticle catalyses the axial growth of a nanowire of radius r_1 and length L which has total volume $\pi r_1^2 L$. The volume is also determined by the integrated flux given by $AF_1\tau_1$ where F_1 and τ_1 are respectively the incident flux in, and total time of, the first phase of growth. In the second growth phase a shell of volume $(\pi r_2^2 - \pi r_1^2)L$ grows where r_2 is the radius of the core–shell nanowire. This volume is then given by $AF_2\tau_2$ where F_2 and τ_2 are the flux in and time of the second growth phase. Combining these relations gives a prediction for the relative radii of the core (r_1) and the outer shell (r_2):

$$r_2 = \left(\sqrt{1 + \frac{F_2\tau_2}{F_1\tau_1}}\right) r_1. \quad (2)$$

The radii data can be fitted with a line through the origin (figure 3(c)), consistent with this model. The gradient is 1.52 which implies $F_2\tau_2/F_1\tau_1 = 1.31$, very close to the experimental value of 1.38. This excellent agreement, even for this simple model, supports the proposed mode of heterostructure growth.

The thin shell in sample A was sufficient to affect the PL spectra of core–shell nanowires (figure 4). Compared to an uncoated control, the PL transitions across the ZnO band gap are stronger, whilst those from the defects are weaker. Whilst these ZnMgO shells are not thick enough to emit a measurable PL signal directly, they clearly modulate recombination at surface defects. We have reported studies on these surface states in plain ZnO nanowires [17].

The ZnMgO shell passivates the nanowire surface as has been seen for core–shell ZnO/Al_2O_3 nanowires [18] due to the dielectric shell screening the charges of surface states and reducing the band-bending at the nanowire surface. The increase in PL emission is also seen for nanowires with cubic MgO or ZnMgO shells [10], indicating a general mechanism by which a wide-band shell may suppress band-bending and thus increase luminescence efficiency. Furthermore, as XRD measurements show no evidence of rock-salt phases these shells are wurtzite and are therefore compatible with a fully epitaxial interface which may be achieved with further growth

refinements. Epitaxial shells with small lattice mismatch are compatible with defect free shells, important since shell defects have been shown to degrade optical properties [6].

4. Conclusion

ZnO/ZnMgO heterostructure nanowires were grown by plasma-assisted gold-catalysed MBE via the VLS mechanism. PL and STEM-EDX studies reveal the relationship between the structure and the electronic properties. Axial heterostructures are hard to access due to diffusion of Mg into the ZnO lattice at elevated temperatures and catalyst solidification at lower temperatures. In the future, catalysts with lower melting points such as tin may be used to grow these structures. However, core–shell heterostructures can be grown via a two-stage process: a ZnO nanowire core is grown axially by VLS before cooling the sample to a temperature below the melting point of the catalyst to grow the ZnMgO shell. PL measurements show an increase in optical quality of heterostructure nanowires over bare nanowires with more intense inter-band emission and a less intense defect peak. EDX maps show that nanowires grow with the core–shell structure and that the thickness of the nanowire shells varies systematically. The growth techniques reported here will aid future growth of heterostructures of ZnO/ZnMgO and other chemistries.

Acknowledgments

The authors gratefully acknowledge financial support from EPSRC grant reference EP/K035274/1 (MSPS and ERW) and EP/H005544/1 (PAW and OWK).

ORCID iDs

O W Kennedy https://orcid.org/0000-0002-1945-960X
M S P Shaffer https://orcid.org/0000-0001-9384-9043
P A Warburton https://orcid.org/0000-0002-3483-1545

References

[1] Conesa-Boj S, Li A, Koelling S, Brauns M, Ridderbos J, Nguyen T T, Verheijen M A, Koenraad P M, Zwanenburg F A and Bakkers E P 2017 Boosting hole mobility in coherently strained [110]-oriented Ge-Si core–shell nanowires *Nano Lett.* **17** 2259–64

[2] Boland J L *et al* 2015 Modulation doping of GaAs/AlGaAs core–shell nanowires with effective defect passivation and high electron mobility *Nano Lett.* **15** 1336–42

[3] Lauhon L J, Gudiksen M S, Wang D and Lieber C M 2002 Epitaxial core–shell and core-multishell nanowire heterostructures *Nature* **420** 57

[4] Ohtomo A, Kawasaki M, Koida T, Masubuchi K, Koinuma H, Sakurai Y, Yoshida Y, Yasuda T and Segawa Y 1998 Mg_xZn_{1-x} O as a II–VI widegap semiconductor alloy *Appl. Phys. Lett.* **72** 2466–8

[5] Tampo H *et al* 2008 Polarization-induced two-dimensional electron gases in ZnMgO/ZnO heterostructures *Appl. Phys. Lett.* **93** 202104

[6] Thierry R, Perillat-Merceroz G, Jouneau P-H, Ferret P and Feuillet G 2012 Core–shell multi-quantum wells in ZnO/ZnMgO nanowires with high optical efficiency at room temperature *Nanotechnology* **23** 085705

[7] Park W I, Yi G-C, Kim M Y and Pennycook S J 2003 Quantum confinement observed in ZnO/ZnMgO nanorod heterostructures *Adv. Mater.* **15** 526–9

[8] Jang E-S, Bae J Y, Yoo J, Park W I, Kim D-W, Yi G-C, Yatsui T and Ohtsu M 2006 Quantum confinement effect in ZnO/ $Mg_{0.2}Zn_{0.8}O$ multishell nanorod heterostructures *Appl. Phys. Lett.* **88** 023102

[9] Cao B Q, Zúñiga-Pérez J, Boukos N, Czekalla C, Hilmer H, Lenzner J, Travlos A, Lorenz M and Grundmann M 2009 Homogeneous core/shell ZnO/ZnMgO quantum well heterostructures on vertical ZnO nanowires *Nanotechnology* **20** 305701

[10] Ahn C H, Mohanta S K, Kong B H and Cho H K 2009 Enhancement of band-edge emission of ZnO from one-dimensional ZnO/MgZnO core/shell nanostructures *J. Phys. D: Appl. Phys.* **42** 115106

[11] Heo Y W, Kaufman M, Pruessner K, Siebein K N, Norton D P and F Ren 2005 ZnO/cubic (Mg, Zn) O radial nanowire heterostructures *Appl. Phys.* A **80** 263–6

[12] Kennedy O W, Coke M L, White E R, Shaffer M S P and P A Warburton 2018 MBE growth and morphology control of ZnO nanobelts with polar axis perpendicular to growth direction *Mater. Lett.* **212** 51–3

[13] Isakov I, Panfilova M, Sourribes M J L and Warburton P A 2013 Growth of ZnO and ZnMgO nanowires by Au-catalysed molecular-beam epitaxy *Phys. Status Solidi* c **10** 1308–13

[14] Ohtomo A, Shiroki R, Ohkubo I, Koinuma H and Kawasaki M 1999 Thermal stability of supersaturated Mg_xZn_{1-x} O alloy films and Mg_xZn_{1-x} O/ZnO heterointerfaces *Appl. Phys. Lett.* **75** 4088–90

[15] Ding Y, Gao P X and Wang Z L 2004 Catalyst- nanostructure interfacial lattice mismatch in determining the shape of VLS grown nanowires and nanobelts: a case of Sn/ZnO *J. Am. Chem. Soc.* **126** 2066–72

[16] Dhaka V *et al* 2013 Aluminum-induced photoluminescence red shifts in core–shell GaAs/Al_xGa_{1-x} As nanowires *Nano Lett.* **13** 3581–8

[17] Kennedy O W, White E R, Howkins A, Williams C K, Boyd I W, Warburton P A and Shaffer M S P 2019 Mapping the origins of luminescence in ZnO nanowires by STEM-CL *J. Phys. Chem. Lett.* **10** 386–92

[18] Richters J P, Voss T, Kim D S, Scholz R and Zacharias M 2008 Enhanced surface-excitonic emission in ZnO/Al_2O_3 core–shell nanowires *Nanotechnology* **19** 305202